Research Article Vol. 32, No. 22 / 21 Oct 2024 / Optics Express 40030
Optics EXPRESS

Sagnac-witnessed laser deflection is an ultra-sensitive acoustic detector

LOGAN E. HILLBERRY,* ZACHARY I. E. MORRISON, RYAN J. SCHLIMME, AND MARK G. RAIZEN

Department of Physics, The University of Texas at Austin, 2515 Speedway, Austin, TX 78712, USA
*lhillber@utexas.edu

Abstract: Laser-deflection-based acoustic sensing is known for high bandwidth but low sensitivity. By embedding the sensing laser within a Sagnac interferometer and incorporating split-beam detection—originally developed for optical trapping microscopy—we demonstrate sensitive acoustic detection in air with a 2 MHz bandwidth. In a direct comparison, our method far-exceeds performance metrics of a state-of-the-art, commercially-available, high-bandwidth microphone. In upcoming large-volume-bubble-chamber searches for dark matter, our method could replace traditional acoustic sensors confined to the chamber's exterior where signals are weakest.

© 2024 Optica Publishing Group under the terms of the Optica Open Access Publishing Agreement

1. Introduction

It has long been known that sound influences the propagation of light [1,2]. Physically, the pressure variations of a sound wave induce proportional variations in density and hence also refractive index. For example, optical diffraction from ultrasonic standing waves forms the basis of acousto-optical laser frequency modulation and beam steering. Recently, high power lasers have been deflected by ultrasound in air using this effect [3]. By the same physics, light may be used to quantify sound in a variety of ways [4,5]. Acoustically driven variations of a medium's refractive index may be detected interferometrically by comparing the phase of a light beam passing through a sound wave to that of an otherwise-identical reference beam [6]. Separate from interferometric methods, sound may be detected by small deflections of a probe beam passing through a sound wave, partially masked by a knife edge, and incident upon a fast photodiode. This technique is often called *probe-beam deflection* [4,7], but it is also known as gas-coupled laser acoustic detection [8,9] or optical probing of the acoustic refractive-index gradient [10]. Early uses for this technique studied the relaxation dynamics in fluids after passage of a shock wave [11]. Later refinements used a focused laser as the probe beam. A focused beam greatly enhanced the detection bandwidth that scales as the speed of sound divided by the probe beam's width. Such refinements enabled resolution of sound speeds in liquids [7], ultrasonic nozzle flow [12], and shock wave profiles [13].

Like related Schlieren imaging techniques – which can be traced back to the work of R. Hooke in 1672 [14] – the probe beam deflection signal is proportional to the gradient of acoustic pressure, integrated along the probe beam's path. In fact, the deflection signal is proportional to the pressure gradient for *plane* acoustic waves; for spherical waves, corrections can account for acoustic wavefront curvature [15]. Modern probe-beam deflection setups typically use a quadrant photodiode in place of a knife edge and single-photodiode. The quadrant photodiode signal of acoustically driven probe-beam deflections enables all-optical photoacoustic microscopy [16], non-contact defect detection [9], and determination of sound's propagation direction. [17].

In this article, we report on an apparatus improving the state-of-the art in probe beam deflection for acoustic sensing. Our approach, depicted schematically in Fig. 1(a) and further detailed in Supplement 1, consists of two unique features. First, inspired by optical trapping microscopy

#530768 https://doi.org/10.1364/OE.530768
Journal © 2024 Received 22 May 2024; revised 15 Aug 2024; accepted 16 Aug 2024; published 18 Oct 2024

Optics EXPRESS

methods for monitoring Brownian particles [18–20], we employ a cut-mirror and balanced-photodetector to measure the probe beam's acoustically-driven deflections. This method, which we call *split-beam* (SB) detection, allows the use of small, and hence fast, photodiodes (like the traditional knife-edge technique) while still rejecting common-mode relative intensity noise (like the quadrant detector technique). Second, we align our probe beam as a Sagnac interferometer [21,22] and detect deflections at the system's dark port. We say the Sagnac interferometer is a *witness* to beam deflections, leading to quantifiable metrological gain. We predict interference patterns at the cut mirror position and the resulting SB signal using ray tracing simulations in Fig. 1(b) and (c) (see Supplement 1 for simulation details).

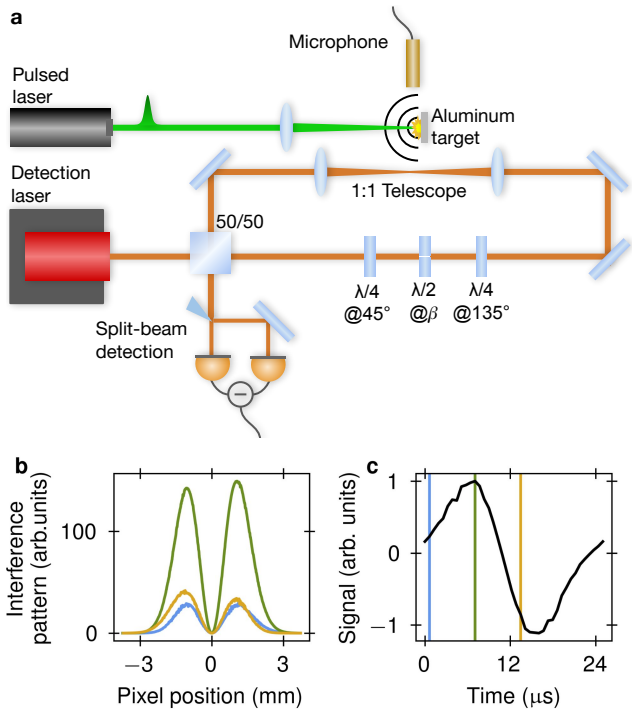

Fig. 1. The Sagnac-witnessed laser deflection for acoustic sensing. (a) Schematic of the setup. The detection laser beam is divided by a 50/50 beamsplitter. The resulting beams traverses counter-propagating loops, forming a Sagnac interferometer. One arm of the interferometer is aligned through a 1:1 telescope formed by identical 150 mm focal length lenses. Another arm features a quarter-wave, half-wave, quarter-wave-plate triplet used to adjust the relative phase between the two beams. A D-shaped cut mirror and balanced photodetector are aligned at the dark port of the interferometer for split-beam detection. To generate test sounds, a pulsed excitation laser is focused onto an aluminum target positioned between the Sagnac's telescope arm and a high-bandwidth reference microphone. When the beamsplitter is removed, the Sagnac effect is destroyed and the system resembles a traditional beam-deflection-based acoustic sensor. (b) Example interference patterns at the cut mirror's position, simulated by ray tracing. Colors correspond to different times during excitation with a 40 kHz sinusoidal refractive index gradient across the telescope arm. (c) The simulated split-beam signal for one excitation cycle. Vertical lines mark specific times and are color coded with the interference patterns shown in (b).

Beyond their traditional use as inertial sensors [22], Sagnac interferometers have demonstrated picoradian $/\sqrt{\text{Hz}}$-sensitivity to mirror-driven beam deflection [23,24], technical noise reduction [25,26], ultra-fast response to temperature-induced refractive index variations [27], enhanced

Optics EXPRESS

beam-deflection-based photothermal spectroscopy [28], and enhanced position monitoring of optically trapped microspheres [29,30]. Theoretically, the Sagnac enhancement may be understood as classical wave interference [29] or as a quantum weak-value measurement [24,26]. Optical-fiber-based Sagnac interferometers have been used for several years as hydrophones and surface acoustic wave sensors [31–34]. There, the detection mechanism is based on strain-induced refractive index changes within kilometer-length fiber coils. Our method relies on beam deflection within a free-space Sagnac loop and our emphasis is on ultrasonic measurements in air. Despite this relevant prior work, Sagnac-enhanced detection of acoustically driven probe beam deflection has thus far remained unexplored.

Though our proof-of-principle experiments take place in air, it is quite straight forward to pass the probe beam through a fluid-filled chamber [28]. One particularly promising application is towards dark matter detection in a bubble chamber. Over the past decade, bubble chamber searches for weakly-interacting massive particles (WIMPs), a family of theoretical dark matter candidates, have provided the tightest direct-detection constraints on spin-dependent WIMP-proton scattering cross sections [35,36]. Critical to this technique's sensitivity is acoustic discrimination between alpha-particle recoils and single-proton recoils [37,38]. Lead zirconate titante piezoelectric acoustic transducers epoxied to the outer chamber wall veto alpha recoil events. However, this technique grows less sensitive as the chamber volume grows, and planning for a tonne-scale chamber is underway, promising a >4× increase in detector volume compared to the current apparatus [39]. To address the loss of acoustic sensitivity, we propose our acoustic detection scheme replace surface-confined piezoelectric transducers. Our detection laser (or arrays of them) could be passed through the chamber such that bubble events are, on average, approximately 100 times closer to the detection point. Assuming only geometric loss, the acoustic amplitude at our sensor would be 10^4 times larger. The existing technique also suffers loss due to acoustic reflection at the impedance-mismatched boundary, which we crudely estimate as a factor of 10. Therefore, our probe beam could be subject to a 10^5 times greater acoustic impulse, as compared to the outer-surface-confined sensors, for the same bubble event.

In the remainder of this article, we discuss experiments undertaken to characterize our Sagnac-enhanced, probe-beam deflection acoustic sensor. Using laser ablation as a high-frequency-content impulsive test sound, we compare the bandwidths of traditional and Sagnac-enhanced beam-deflection measurements. The traditional measurement is made by simply removing the beamsplitter in our setup, but maintaining our SB detection. For reference, signals are compared to a calibrated, high-bandwidth gas-coupled microphone. Then, using a continuous 40 kHz tone, we compare signal-to-noise ratios (SNRs) between our microphone, Sagnac-enhanced SB, and Sagnac-enhanced single-photodiode (SPD) measurements. Taken together, our experiments quantify the meteorological gain afforded by SB detection and Sagnac interferometry.

2. Results

Pulsed lasers provide a convenient and tuneable impulsive acoustic source [40–43]. When a focused pulse impinges on a metal surface, at least two distinct regimes of sound generation are possible. At lower laser intensities, the material responds thermoelastically to the sudden laser-induced heating, sourcing a relatively weak acoustic impulse [44]. Beyond some critical fluence, usually a few J/cm^2 for nanosecond laser pulses [45–47], the material is vaporized and ionized in a complex process known as laser ablation. Compared to the thermoelastic response, laser ablation sources a weak shock wave with significantly higher peak pressures and a universal N-shape [48]. We focus a variable-energy pulsed laser (pulse width 5 ns, wavelength 532 nm) to approximately $100\mu m$ on an aluminum target to generate either ablative or thermoelastic acoustic impulses as test sounds.

Figure 2 reports a typical laser ablation signal as measured by (i) a calibrated (0.68 mV/Pa nominal sensitivity) high-bandwidth (200 kHz) microphone, (ii) traditional beam deflection

Optics EXPRESS

measured with SB detection, and (iii) Sagnac-enhanced SB detection. The laser deflection signals are shown in physical units by accounting for the system's theoretical response function [15] and rescaling to match the slower trough portion of the calibrated microphone's signal (see Supplement 1 for details).

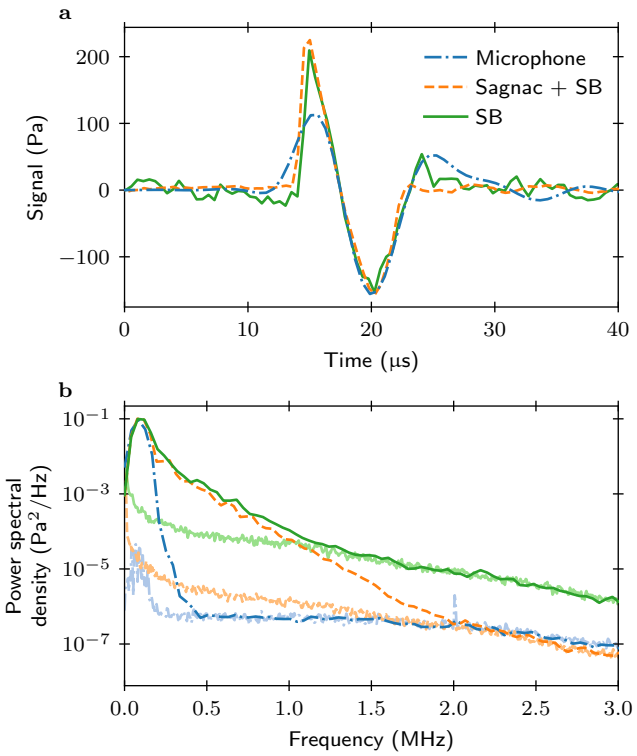

Fig. 2. Estimating bandwidth using laser ablation acoustics. (a) Example single-shot time-domain signals as recorded by the microphone (blue, dot-dashed), split-beam (SB) sensing of probe beam deflection (green, solid) and Sagnac-enhanced SB detection (orange, dashed). (b) Power spectral densities (averaged over 50 shots) of the signals (darker curves) in (a) compared to noise (lighter curves). Colors are coordinated with panel (a). The pulsed laser energy is 7 mJ so the fluence at the target is approximately 89 J/cm^2.

Figure 2(a) shows the signal in the time domain lasts approximately 10μs. The microphone's limited bandwidth significantly distorts the signal's leading edge. The microphone resolves a longer initial rise time – defined here as the time it takes for the signal to change from 10% to 90% of its peak value – of 2.0(3)μs and a lower peak pressure of 115(3) Pa. Numbers in parentheses report uncertainty in the last digits of quoted results. The quoted results reflect the average, while uncertainty is the standard deviation, of values measured across 50 shots. By comparison, laser deflection measured with SB detection registers a faster initial rise time of 0.8(4)μs and a higher peak pressure of 270(29) Pa. The Sagnac-enhanced SB detection resolves a peak pressure of 250(12) Pa and a rise time of 0.50(4)μs.

In Fig. 2(b), the power spectral densities of the same signals quantifies their frequency content in comparison to each sensor's self-noise. In the frequency domain, we estimate the bandwidth of the sensor as the point where the signal decays to the noise floor. For the microphone, this method roughly agree with the manufacturer's stated bandwidth of 200 kHz. For SB detection, the bandwidth is at least 1.2 MHz alone or 2.0 MHz with Sagnac enhancement.

Optics EXPRESS

Due to its greater high-frequency acoustic sensitivity, the Sagnac-enhanced SB acoustic detection can measure signals that the microphone cannot. This is demonstrated in Fig. 3 where a weak, thermoelastic acoustic impulse is simultaneously measured via probe beam deflection, but obscured by noise in the microphone. Figure 3(a) shows the Sagnac-enhanced SB signal, which last approximately 2.5μs. We show raw voltage signals, but the peak pressure in the acoustic impulse is estimated to be on the order of 1 Pa based on the microphone's sensitivity and observed noise levels in Fig. 3(b). Even upon averaging 10 independent shots (black lines), the microphone does not resolve the thermoelastic acoustic impulse. Meanwhile, the Sagnac-enhanced SB detection resolves the same impulse at the single-shot level, albeit with a signal-to-noise-ratio (SNR) on the order of unity.

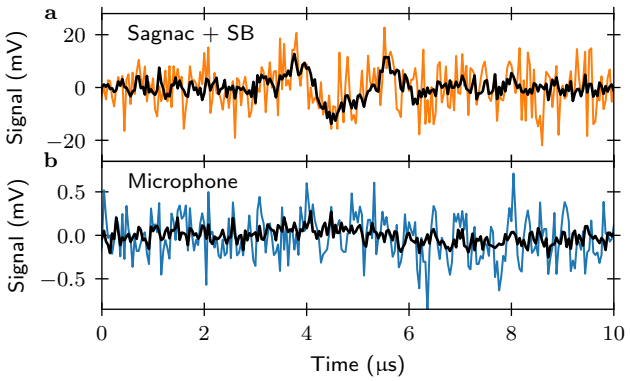

Fig. 3. Minimum-detectable thermoelastic acoustic signal. (a) The raw voltage signal from the Sagnac setup, measured with split beam (SB) detection. (b) The microphone's raw signal. In both panels, the black line reflects a 10-shot average. The pulsed laser energy is 0.063 mJ, so the fluence at the target is approximately 0.81 J/cm^2.

As demonstrated previously in Sagnac-enhanced photothermal spectroscopy [28], the Sagnac interferometer offers an alternative beam deflection sensing modality. Split-beam detection measures the power imbalance between two halves of the laser mode exiting the interferometer's dark port. In addition to asymmetry in the interference pattern, the total power exiting the dark port is modulated by the passage of acoustic waves. Therefore, focusing the dark port's output onto a single-photodiode (SPD) also provides acoustic sensitivity. For this sensing modality, we find it necessary to optimize the relative phase between the two Sagnac beams so that the dark port is slightly bright. Alternatively, the Sagnac can be intentionally misaligned by an optimal, beam-size-dependant amount [28]. To adjust the Sagnac phase, we use two quarter-wave plates surrounding a half waveplate in one arm of the interferometer loop [23] (see Fig. 1(a)). The two quarter wave plates' fast axes are at 45° and 135° with respect to the input beams polarization, respectively. As the half-waveplate's fast axis is rotated by β the relative phase between the two Sagnac beams is adjusted by $\theta = 4\beta$. Even with careful alignment, the dark port is never completely dark. We estimate the Sagnac phase in our system by measuring the power entering the interferometer P_{in} and the power exiting the dark port P_{out}. We achieve an extinction ratio of $P_{\text{out}}/P_{\text{in}} \approx 1/100$ from which we estimate the minimum Sagnac phase as $\theta = 2 \arcsin \sqrt{P_{\text{out}}/P_{\text{in}}} = 11.5°$.

In Fig. 4 we compare Sagnac-enhanced SB and SPD detection in terms of SNR. For this experiment, we use as the sound source a 40 kHz piezo buzzer driven at its resonant frequency by a 1 V peak-to-peak sine wave. The SNR for both interferometric detection schemes is measured at various Sagnac phase angles θ and compared to the microphone's SNR. The Sagnac-enhanced SB detection method achieves a typical max SNR of 25 dB, comparable to the microphone. The

Optics EXPRESS

SNR decays rapidly upon increasing θ as -2.7(2) dB per degree. Conversely, the SPD detecion method exhibits a broadly peaked SNR of approximately 13 dB at $\theta = 30°$.

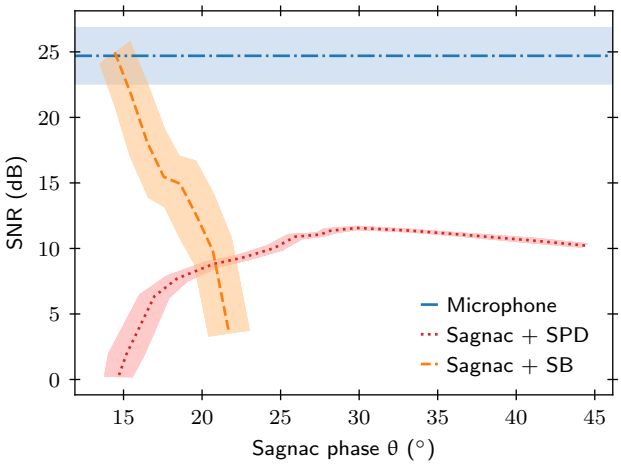

Fig. 4. Signal to noise ratio comparison. A continuous 40 kHz acoustic stimulus is measured approximately 1 cm from the source using three methods. The microphone (blue, dot-dashed) achieves an SNR of 25(2) dB. Uncertainty, represented by the shaded band, expresses the standard deviation of 100 trials. Sagnac-enhanced split beam (SB, orange, dashed) and single-photodiode (SPD, red, dotted) detection SNRs represent accumulated statistics over 5 Sagnac phase scans across three days of testing. Error bands account for uncertainty in the phase and SNR at each setting of the 5 scans. The best single SNR measurement was 27(2) dB, achieved by the Sagnac+SB method with a phase of 11.5°.

3. Conclusions

In this article, we have proposed and demonstrated a novel laser-based acoustic detection scheme. By combining a Sagnac interferometer and split-beam detection we achieve high bandwidth and high signal-to-noise ratio acoustic detection in air.

We now provide a summary analysis of our data. First, using laser ablation as a sound source, we demonstrate the Sagnac interferometer enables a 67% increase in bandwidth and an order of magnitude lower statistical fluctuation in acoustic-impulse rise time compared to split-beam detection alone. Second, using weak thermoelastic acoustic signals and comparison to a calibrated microphone, we estimate our system's noise-equivalent pressure is on the order of 1 Pa at 400 kHz. The 400 kHz frequency is estimated by the inverse of the weak signal's 2.5μs duration. Under the same stimulus, the microphone registers only noise with a signal amplitude less than 0.5 mV, or pressure on the order of 1 Pa within its 200 kHz bandwidth. Assuming that there is not significant additional noise in the 200 kHz to 400 kHz band leads us to the above noise equivalent pressure estimate. More quantitatively, the integral of the noise spectrum (Fig. 2(b), light orange curve) to the 1/2-power gives a noise-equivalent pressure of 2.6 Pa at 400 kHz (3.0 Pa at 2 MHz). Finally, split-beam, as compared to single-photodiode, deflection measurements afford more than 10 dB enhancement to signal-to-noise ratios after optimizing the Sagnac beams' relative phase for each measurement.

Our demonstration has taken place in air, but our methods apply equally well to other media: Bandwidths scale with the medium's speed of sound and sensitivity scales with the rate at which the medium's refractive index changes with pressure. Applying our methods to existing laser-deflection-based measurements could improve, e.g., spatial resolution of all-optical photoacoustic microscopy, sensitivity of all-optical photoacoustic- and photothermal-spectroscopy,

Optics EXPRESS

and reliability of acoustically transduced noncontact defect detection in solids. A particularly promising application of our method is to acoustic discrimination in bubble-chamber searches for dark matter.

Acknowledgments. M.G. Raizen acknowledges support from the Sid. W. Richardson Foundation.

Disclosures. The authors declare no conflicts of interest.

Data availability. Data underlying the results presented in this paper are not publicly available at this time but may be obtained from the authors upon reasonable request.

Supplemental document. See Supplement 1 for supporting content.

References

1. R. Lucas and P. Biquard, "Propriétés optiques des milieux solides et liquides soumis aux vibrations élastiques ultra sonores," J. Phys. Radium **3**(10), 464–477 (1932).
2. P. Debye and F. Sears, "On the scattering of light by supersonic waves," Proc. Natl. Acad. Sci. U.S.A. **18**(6), 409–414 (1932).
3. Y. Schrödel, C. Hartmann, J. Zheng, *et al.*, "Acousto-optic modulation of gigawatt-scale laser pulses in ambient air," Nat. Photonics **18**(1), 54–59 (2024).
4. G. Wissmeyer, M. A. Pleitez, A. Rosenthal, *et al.*, "Looking at sound: optoacoustics with all-optical ultrasound detection," Light: Sci. Appl. **7**(1), 53 (2018).
5. B. Fu, Y. Cheng, and C. Shang, "Optical ultrasound sensors for photoacoustic imaging: a narrative review," Quant Imaging Med Surg **12**(2), 1608–1631 (2022).
6. Z. Rehman, A. Raza, and H. Qayyum, "Characterization of laser-induced shock waves generated during infrared laser ablation of copper by the optical beam deflection method," Appl. Opt. **61**(29), 8606–8612 (2022).
7. W. Zapka and A. Tam, "Photoacoustic pulse generation and probe-beam deflection for ultrasonic velocity measurements in liquids," Appl. Phys. Lett. **40**(4), 310–312 (1982).
8. J. N. Caron, Y. Yang, J. B. Mehl, *et al.*, "Gas-coupled laser acoustic detection at ultrasonic and audio frequencies," Rev. Sci. Instrum. **69**(8), 2912–2917 (1998).
9. M.-S. Gulino, M. Bruzzi, J. N. Caron, *et al.*, "Non-contact ultrasonic inspection by gas-coupled laser acoustic detection (gclad)," Sci. Rep. **12**(1), 87 (2022).
10. A. C. Tam, "Applications of photoacoustic sensing techniques," Rev. Mod. Phys. **58**(2), 381–431 (1986).
11. E. Resler Jr and M. Scheibe, "Instrument to study relaxation rates behind shock waves," J. Acoust. Soc. Am. **27**(5), 932–938 (1955).
12. G. W. Faris and R. L. Byer, "Quantitative three-dimensional optical tomographic imaging of supersonic flows," Science **238**(4834), 1700–1702 (1987).
13. G. Davidson and D. Emmony, "A schlieren probe method for the measurement of the refractive index profile of a shock wave in a fluid," J. Phys. E: Sci. Instrum. **13**(1), 92–97 (1980).
14. J. Rienitz, "Schlieren experiment 300 years ago," Nature **254**(5498), 293–295 (1975).
15. J. Diaci, "Response functions of the laser beam deflection probe for detection of spherical acoustic waves," Rev. Sci. Instrum. **63**(11), 5306–5310 (1992).
16. S. M. Maswadi, B. L. Ibey, and C. C. Roth, "All-optical optoacoustic microscopy based on probe beam deflection technique," Photoacoustics **4**(3), 91–101 (2016).
17. R. A. Barnes, S. Maswadi, R. Glickman, *et al.*, "Probe beam deflection technique as acoustic emission directionality sensor with photoacoustic emission source," Appl. Opt. **53**(3), 511–519 (2014).
18. T. Li, S. Kheifets, D. Medellin, *et al.*, "Measurement of the instantaneous velocity of a brownian particle," Science **328**(5986), 1673–1675 (2010).
19. S. Kheifets, A. Simha, and K. Melin, "Observation of brownian motion in liquids at short times: instantaneous velocity and memory loss," Science **343**(6178), 1493–1496 (2014).
20. Z. Chen, T. Kuang, and X. Han, "Differential displacement measurement of the levitated particle using d-shaped mirrors in the optical tweezers," Opt. Express **30**(17), 30791–30798 (2022).
21. G. Sagnac, "L'éther lumineux démontré par l'effet du vent relatif d'éther dans un interféromètre en rotation uniforme," Comptes rendus de l'Académie des Sciences **157**, 708–710 (1913).
22. E. J. Post, "Sagnac effect," Rev. Mod. Phys. **39**(2), 475–493 (1967).
23. J. Hogan, J. Hammer, and S.-W. Chiow, "Precision angle sensor using an optical lever inside a sagnac interferometer," Opt. Lett. **36**(9), 1698–1700 (2011).
24. P. B. Dixon, D. J. Starling, A. N. Jordan, *et al.*, "Ultrasensitive beam deflection measurement via interferometric weak value amplification," Phys. Rev. Lett. **102**(17), 173601 (2009).
25. D. J. Starling, P. B. Dixon, A. N. Jordan, *et al.*, "Optimizing the signal-to-noise ratio of a beam-deflection measurement with interferometric weak values," Phys. Rev. A **80**(4), 041803 (2009).
26. A. N. Jordan, J. Martínez-Rincón, and J. C. Howell, "Technical advantages for weak-value amplification: when less is more," Phys. Rev. X **4**(1), 011031 (2014).
27. D. H. Hurley and O. B. Wright, "Detection of ultrafast phenomena by use of a modified sagnac interferometer," Opt. Lett. **24**(18), 1305–1307 (1999).

Optics EXPRESS

28. N. Shiokawa, Y. Mizuno, H. Tsuchiya, *et al.*, "Sagnac interferometer for photothermal deflection spectroscopy," Opt. Lett. **37**(13), 2655–2657 (2012).
29. M. A. Taylor, J. Knittel, and M. Hsu, "Sagnac interferometer-enhanced particle tracking in optical tweezers," J. Opt. **13**(4), 044014 (2011).
30. I. Galinskiy, O. Isaksson, and I. R. Salgado, "Measurement of particle motion in optical tweezers embedded in a sagnac interferometer," Opt. Express **23**(21), 27071–27084 (2015).
31. J. A. Bucaro, H. D. Dardy, and E. F. Carome, "Optical fiber acoustic sensor," Appl. Opt. **16**(7), 1761–1762 (1977).
32. K. Kråkenes and K. Bløtekjaer, "Sagnac interferometer for underwater sound detection: noise properties," Opt. Lett. **14**(20), 1152–1154 (1989).
33. J. Bowers, "Fiber-optical sensor for surface acoustic waves," Appl. Phys. Lett. **41**(3), 231–233 (1982).
34. P. R. Hoffman and M. G. Kuzyk, "Position determination of an acoustic burst along a sagnac interferometer," J. Lightwave Technol. **22**(2), 494–498 (2004).
35. C. Amole, M. Ardid, and D. M. Asner, "Dark matter search results from the pico-2l c_3f_8 bubble chamber," Phys. Rev. Lett. **114**(23), 231302 (2015).
36. C. Amole, M. Ardid, and I. J. Arnquist, "Dark matter search results from the PICO–60 c_3f_8 bubble chamber," Phys. Rev. Lett. **118**(25), 251301 (2017).
37. F. Aubin, M. Auger, and M. Genest, "Discrimination of nuclear recoils from alpha particles with superheated liquids," New J. Phys. **10**(10), 103017 (2008).
38. E. Behnke, J. Behnke, and S. Brice, "Improved limits on spin-dependent wimp-proton interactions from a two liter cf 3 i bubble chamber," Phys. Rev. Lett. **106**(2), 021303 (2011).
39. C. B. Krauss and for the PICO Collaboration, "Pico-60 results and pico-40l status," J. Phys.: Conf. Ser. **1468**(1), 012043 (2020).
40. I. Kajiwara, R. Akita, and N. Hosoya, "Damage detection in pipes based on acoustic excitations using laser-induced plasma," Mechanical Systems and Signal Processing **111**, 570–579 (2018).
41. L. V. Wang and S. Hu, "Photoacoustic tomography: in vivo imaging from organelles to organs," Science **335**(6075), 1458–1462 (2012).
42. Q. Qin and K. Attenborough, "Characteristics and application of laser-generated acoustic shock waves in air," Applied Acoustics **65**(4), 325–340 (2004).
43. L. Hillberry and M. Raizen, "Optically trapped microspheres are high-bandwidth acoustic transducers," Phys. Rev. Appl. **21**(1), 014031 (2024).
44. M. W. Sigrist, "Laser generation of acoustic waves in liquids and gases," J. Appl. Phys. **60**(7), R83–R122 (1986).
45. M. Stafe, I. Vladoiu, and I. M. Popescu, "Impact of the lasr wavelength and fluence on the ablation rate of aluminium," Cent. Eur. J. Phys. **6**(2), 327–331 (2008).
46. I. Vladoiu, M. Stafe, C. Negutu, *et al.*, "Nanopulsed ablation rate of metals dependence on the laser fluence and wavelength in atmospheric air," UPB Scientific Bulletin, Series A: Applied Mathematics and Physics **70**(4), 119–126 (2008).
47. C. Porneala and D. A. Willis, "Observation of nanosecond laser-induced phase explosion in aluminum," Appl. Phys. Lett. **89**(21), 211121 (2006).
48. T. W. Murray and J. W. Wagner, "Laser generation of acoustic waves in the ablative regime," J. Appl. Phys. **85**(4), 2031–2040 (1999).

128.62.53.103 {ts '2024-10-21 16:46:52'}